Isogeometric Analysis for Electromagnetic Problems

Rafael Vázquez and Annalisa Buffa

Istituto di Matematica Applicata e Tecnologie Informatiche, National Research Centre (CNR), Pavia I-27100, Italy

Isogeometric analysis (IGA) is a novel discretization method, introduced by Hughes *et al.*, which is based on nonuniform rational B-splines (NURBS). Among other features, IGA uses directly the geometry description coming from computer-aided design software without approximation, and the analysis is performed using shape functions of variable (possibly high) regularity. In this paper we propose a new discretization scheme based on continuous B-splines, adapting the IGA to the solution of Maxwell's equations. We present extensive numerical results to show that our scheme is free of spurious modes, and that it approximates singular solutions in domains with reentrant corners and edges.

***Index Terms*—Edge elements, eigenvalue problem, isogeometric analysis, Maxwell equations.**

I. Introduction

In THIS paper we focus on the problem of solving Maxwell's eigenvalues in a cavity

Find $\omega \in \mathbb{R}$ *and* $\mathbf{E} \in \mathbf{H}_0(\mathbf{curl};\Omega)$, $\mathbf{E} \neq \mathbf{0}$, *satisfying*

$$(\mu^{-1}\mathbf{curl}\,\mathbf{E}, \mathbf{curl}\,\mathbf{v}) = \omega^2(\epsilon\mathbf{E}, \mathbf{v}) \quad \forall \mathbf{v} \in \mathbf{H}_0(\mathbf{curl};\Omega) \tag{1}$$

where $\mathbf{H}_0(\mathbf{curl};\Omega)$ is the space of square integrable functions, defined in the physical domain Ω, such that their curl is also square integrable, and their tangential component is zero on the boundary.

It is known that the solution of (1) with nodal finite elements produces an approximation with spurious modes in nonconvex geometries. Instead, edge elements provide a solution which is free of spurious modes and that approximates singular solutions in nonconvex geometries. However, the electromagnetic fields computed with edge elements are discontinuous, and in recent years some methods have been introduced in order to discretize the equations with continuous finite elements (see, e.g., [1] and [2]).

In [3] the concept of isogeometric analysis (IGA) was introduced with the aim of bridging the gap between computer-aided design (CAD) and the finite element method. Loosely speaking, in IGA the space of nonuniform rational B-Splines (NURBS) describing the geometry is also used as the space of trial and test functions in the discrete variational formulation, i.e., an isoparametric concept is adopted. The main advantage of this approach is that *the geometry is exactly described at the coarsest level*, and mesh refinement is done without affecting the geometry. Moreover, NURBS basis functions have higher continuity than usual finite elements. Following the ideas of [3], in this paper we present a new numerical technique, based on (nonrational) B-splines, for the numerical solution of problem (1) with continuous functions.

Manuscript received December 17, 2009; revised February 22, 2010; accepted February 23, 2010. Current version published July 21, 2010. Corresponding author: R. Vázquez (e-mail: vazquez@imati.cnr.it).

Color versions of one or more of the figures in this paper are available online at http://ieeexplore.ieee.org.

Digital Object Identifier 10.1109/TMAG.2010.2044563

II. B-Splines Spaces

In one dimension, B-splines basis functions of order m are constructed from an open knot vector

$$\Xi = \{0 = \xi_1 \leq \xi_2 \leq \cdots \leq \xi_{n+m} = 1\} \tag{2}$$

where the *open* nomenclature means that the first and last knots are repeated m times. Using the iterative procedure described in [3], from the knot vector we can construct n B-splines of degree $p = m - 1$. These B-splines are nonnegative piecewise polynomials which form a partition of unity. The regularity of the basis functions is controlled by the multiplicity of the knots: if the multiplicity of a knot is equal to r, then the basis functions have $p - r$ continuous derivatives at that knot. The maximum regularity is acquired when the knot appears only once, which yields $p - 1$ continuous derivatives in that knot.

In two and three dimensions the definition of B-splines is easily generalized by tensor products. We will only explain the 3-D case, the 2-D one being analogous. Let us consider three knot vectors Ξ_1, Ξ_2, and Ξ_3 which define a mesh in the parametric domain $\Omega_0 = (0,1)^3$. The B-splines basis functions are then defined as $B_{ijk}(x,y,z) := B_i(x)B_j(y)B_k(z)$, where B_i, B_j, and B_k are constructed from the knot vectors Ξ_1, Ξ_2, and Ξ_3, respectively. These B-splines essentially satisfy the same properties we have seen in one dimension.

In order to describe our physical domain through NURBS, we assume that it is the union of n_p subdomains, or patches, in the form $\bar{\Omega} = \cup_{l=1}^{n_p} \bar{\Omega}_l$, with $\Omega_l \cap \Omega_{l'} = \emptyset$, $\forall l \neq l'$. To each subdomain we associate three knot vectors Ξ_1^l, Ξ_2^l, and Ξ_3^l which define the mesh $\mathcal{Q}_H^l(\Omega_0)$ and the corresponding B-spline basis functions B_{ijk}^l in the parametric domain. On the same mesh, NURBS basis functions are defined as $N_{ijk}^l = B_{ijk}^l / w$, where $w \in C^0(\Omega_0)$ is a suitable positive function. Then, the subdomain Ω_l is obtained by a mapping

$$\mathbf{F}_l : \Omega_0 \longrightarrow \Omega_l, \quad \mathbf{x} \longmapsto \mathbf{F}_l(\mathbf{x}) := \sum_{i,j,k} N_{ijk}^l(\mathbf{x})\mathbf{C}_{ijk}^l \tag{3}$$

where $\mathbf{C}_{ijk}^l$ are commonly called control points. We defer the reader to [4] for a discussion on the wide class of domains that can be described by NURBS.

The parametrization $\mathbf{F}_l$ also maps the mesh $\mathcal{Q}_H^l$, defined in the reference domain Ω_0, to a mesh $\mathcal{T}_H^l$ defined in the physical subdomain Ω_l. Since we are only able to treat conforming

meshes, we require that if $\Gamma_{ij} = \bar{\Omega}_i \cap \bar{\Omega}_j$ is not empty, then $\mathcal{T}_H^i|_{\Gamma_{ij}} = \mathcal{T}_H^j|_{\Gamma_{ij}}$. In other words, the two meshes must coincide on the interface Γ_{ij}. Note that these interfaces are not required to be flat, but are in general NURBS manifolds.

The refinement of the mesh in the physical domain is done as in [3]: new knots are inserted in the knot vectors, but the parametrization (3) remains unchanged. In principle this refinement can be done independently in each patch Ω_l, but we require that the refinement preserves the conformity of the mesh at the interfaces, while the treatment of nonconformity deserves further study.

III. Discretization Technique Based on B-Splines

We now introduce a discretization scheme for problem (1) based on B-splines. The main difference with the approach presented in [3] is that the isoparametric approach is relaxed: the parametrization of the domain is written in terms of NURBS, but the discrete spaces are based on nonrational B-splines. However, the main properties of isogeometric analysis are preserved: the geometry is exactly described at the coarsest level mesh, and the method provides smoother solutions than finite elements.

A. Discrete Spaces in the Reference Domain Ω_0

For each subdomain Ω_l, discrete spaces are first defined in the reference domain Ω_0. Let us assume that $\mathcal{Q}_h^l$ is a refinement of the mesh $\mathcal{Q}_H^l$, the mesh where the geometry was defined. Let us denote by $S_l^{p_1,p_2,p_3}$ the space of B-splines of degrees p_1, p_2, and p_3 in the x, y, and z direction, respectively, and constructed on the mesh $\mathcal{Q}_h^l$. On this mesh we define the discrete spaces

$$\begin{aligned} S_l^0 &:= S_l^{p,p,p} \\ S_l^1 &:= S_l^{p-1,p,p} \times S_l^{p,p-1,p} \times S_l^{p,p,p-1} \\ S_l^2 &:= S_l^{p,p-1,p-1} \times S_l^{p-1,p,p-1} \times S_l^{p-1,p-1,p} \\ S_l^3 &:= S_l^{p-1,p-1,p-1}. \end{aligned}$$

With this choice of the spaces, the following diagram holds:

$$S_l^0 \xrightarrow{\mathbf{grad}} S_l^1 \xrightarrow{\mathbf{curl}} S_l^2 \xrightarrow{\mathrm{div}} S_l^3 \tag{4}$$

in the sense that $\ker(\mathbf{curl}) = \mathbf{grad}(S_l^0)$ and $\ker(\mathrm{div}) = \mathbf{curl}(S_l^1)$. The proof of the exactness of this diagram can be found in [5] and [6].

In fact, the discrete spaces S_l^0, S_l^1, and S_l^2 can be understood as a smooth generalization of nodal, edge and facet finite elements, respectively (see [7]). As it is well known, these finite elements satisfy a diagram analogous to (4). Moreover, if the knots are repeated exactly p times, the discrete space S_l^1, defined in the parametric domain Ω_0, coincides exactly with the approximation space for edge elements. One of the advantages of our technique with respect to edge elements is that it allows us to control the regularity of our solutions. For instance, if the domain is formed by several materials with different physical properties, the regularity can be kept at its maximum within each material, and be reduced at the interfaces providing then a discrete solution with discontinuous normal component at material discontinuities.

Remark 3.1: The construction of the spaces in the 2-D case is analogous. In fact, for each mesh $\mathcal{Q}_h^l$ in the unit square we define the spaces

$$S_l^0 := S^{p,p} \quad S_l^1 := S^{p-1,p} \times S^{p,p-1} \quad S_l^2 := S^{p-1,p-1}$$

and a diagram similar to (4) holds.

B. Discrete Spaces in the Physical Domain Ω

After the definition of the discrete spaces in the reference domain Ω_0, it is necessary to define the approximation spaces in the physical domain Ω. We focus on $\mathbf{H}(\mathbf{curl}, \Omega)$ approximation while a general construction is provided in [6]. The space for each subdomain Ω_l is defined through a curl conforming mapping, in the form

$$X_l^1 := \left\{ D\mathbf{F}_l^{-T} \left(\mathbf{u} \circ \mathbf{F}_l^{-1} \right), \mathbf{u} \in S_l^1 \right\}. \tag{5}$$

Then, the approximation space for $\mathbf{H}_0(\mathbf{curl}; \Omega)$ in the whole physical domain Ω, is obtained by gluing the local spaces

$$X^1 = \left\{ \mathbf{u}_h \in \mathbf{H}_0(\mathbf{curl}; \Omega) : \mathbf{u}_h \,|_{\,\Omega_l} \in X_l^1 \right\}. \tag{6}$$

Remark 3.2: The conformity of the meshes at the interfaces Γ_{ij} ensures that the space X^1 is well defined and that it provides a good approximation of $\mathbf{H}_0(\mathbf{curl}; \Omega)$, as soon as the space X_l^1 is a good approximation of $\mathbf{H}_0(\mathbf{curl}; \Omega_l)$, for $l = 1, \ldots, n_p$.

C. Discrete Problem

Once we have introduced the approximating spaces, we can write the discrete version of problem (1). The problem is approximated with a Galerkin method, so the discrete version of the problem reads

Find $\omega \in \mathbb{R}$ *and* $\mathbf{E}_h \in X^1$ *such that*

$$(\mu^{-1}\mathbf{curl}\, \mathbf{E}_h, \mathbf{curl}\, \mathbf{v}_h) = \omega^2 (\epsilon \mathbf{E}_h, \mathbf{v}_h) \quad \forall \mathbf{v}_h \in X^1. \tag{7}$$

Our discretization scheme provides regular eigensolutions and is free of spurious modes. Its theoretical understanding can be found in [6] and here we present numerical tests demonstrating its robustness and efficency.

IV. Numerical Results

We now present several numerical tests to show how our numerical technique performs. We focused our efforts on the approximation of singular solutions in nonconvex geometries, and in domains formed by several materials with different properties. We have taken into account both 2-D and 3-D problems. Our results show that the method performs well in every case, and that it is a promising alternative to edge finite elements.

A. Test 1: The Square Domain

As the first test case we have solved problem (1) in the square, with constant properties $\mu = \epsilon = 1$. The problem has been solved considering different degrees and continuities for the space of solutions. In every case our solution is free of spurious

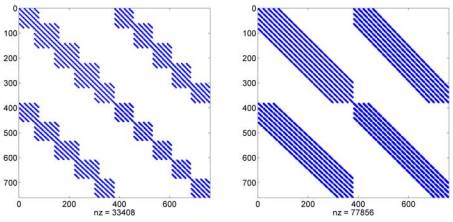

Fig. 1. Sparsity pattern for (left) finite elements and (right) IGA.

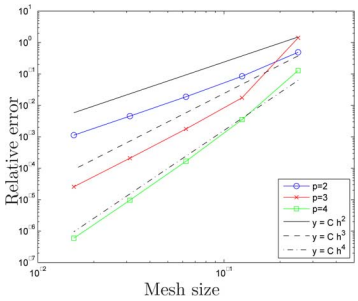

Fig. 2. Convergence rates in the square domain, where h is the mesh size.

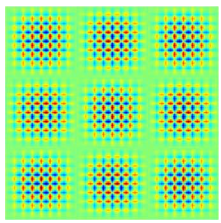

Fig. 3. Computed divergence of the 18th eigenfunction.

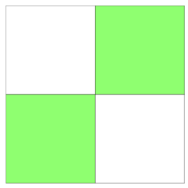

Fig. 4. Check pattern square.

TABLE I
FIRST COMPUTED EIGENVALUES IN THE CHECK PATTERN SQUARE

	IGA, p=2	IGA, p=3	IGA, p=4	Benchmark
D.O.F.	2133	2465	2821	
1^{st} eigv.	3.3175683	3.3175488	3.3175488	3.3175488
2^{nd} eigv.	3.3663352	3.3663227	3.3663236	3.3663242
3^{rd} eigv.	6.1864525	6.1863897	6.1863896	6.1863896
4^{th} eigv.	13.927585	13.926335	13.926323	13.926323
5^{th} eigv.	15.084276	15.083003	15.082991	15.082991
6^{th} eigv.	15.780197	15.778879	15.778866	15.778866
7^{th} eigv.	18.645346	18.643325	18.643297	18.643297
8^{th} eigv.	25.801925	25.797608	25.797533	25.797531
9^{th} eigv.	29.864556	29.852721	29.852410	29.852401
10^{th} eigv	30.549605	30.538166	30.537865	30.537859

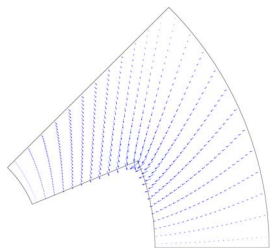

Fig. 5. Curved L-shaped domain. Approximation of the first eigenfunction.

modes, in the sense that the zero eigenvalue is exactly computed. Note that degree elevation provides better and better convergence rate (see Fig. 2) at the cost of very few additional degrees of freedom. Indeed, the number of B-spline basis functions of degree p and continuity k at the knots, in one dimension, is equal to $N(p-k)+1+k$, where N is the number of intervals. Instead, the number of nonzeros of the matrix increases with the continuity index k, because the support of the functions becomes larger. However, the bandwidth of the matrix is always equal to $2p+1$, independently of the regularity. That is, the new nonzero values fill the matrix near the diagonal, but without affecting its band structure. The same is true in two and three space dimensions. This fact is confirmed by the sparsity patterns in the 2-D cases shown in Fig. 1 for $p=4$ and $k=p-1$ (right), and $p=4$ and $k=0$ (left), which corresponds to edge finite elements.

Another advantage of the method with respect to edge finite elements is that it provides continuous solutions, and in particular the divergence of the numerical solution can be computed. In this particular case, the divergence is an oscillating field (see Fig. 3), and it tends to zero with good convergence rates.

B. Test 2: Check Pattern Square

The second test case consists of a square divided in four subdomains, as the one showed in Fig. 4. The magnetic permeability μ is supposed to be equal to one for both materials, whereas the dielectric permittivity ϵ is taken equal to 1 for the first material, and equal to 0.5 for the second one. In order to deal with the discontinuous materials the patches only match with continuity C^0, so that the normal component of the computed solution is discontinuous at the interfaces.

We present in Table I the results of our computation. We notice that, in order to approximate the singularities appearing in the center of the domain, the mesh has been strongly refined near that zone.

C. Test 3: The Curved L-Shaped Domain

The third test concerns with the computation of Maxwell eigenvalues in a nonconvex geometry, in particular a curved L-shaped domain. The geometry is exactly described using NURBS mappings, and it consists of two patches that match with C^0 continuity. We also notice that the coarsest mesh is formed by only two elements which are necessary to obtain the exact geometry. This is a clear advantage with respect to finite elements.

It is known that the first eigenfunction in this domain is singular (see [8]) and nodal finite elements fail to approximate it. Instead, our method approximates this singular function correctly, as it can be seen in Fig. 5.

D. Test 4: Fichera's Corner

Our last test concerns the numerical solution of the cavity problem in Fichera's corner: this is defined as $(-1,1)^3 \setminus [0,1]^3$, i.e., a cube of edge length 2 to which we subtract a cube of edge

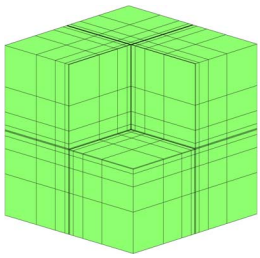

Fig. 6. Mesh for Fichera's corner.

TABLE II
FIRST COMPUTED EIGENVALUES IN FICHERA'S CORNER

	Zaglmayr	Duruflé	IGA, p=3	IGA, p=6
D.O.F.	53982	177720	8421	5436
1^{st} eigv.	3.219994	3.219874	3.219430	3.211175
2^{nd} eigv.	5.880442	5.880419	5.880460	5.880947
3^{rd} eigv.	5.880455	5.880419	5.880460	5.880947
4^{th} eigv.	10.68566	10.68549	10.68662	10.69381
5^{th} eigv.	10.69370	10.69378	10.69496	10.70692
6^{th} eigv.	10.69373	10.69378	10.69496	10.70692
7^{th} eigv.	12.31688	12.31652	12.31795	12.31441
8^{th} eigv.	12.31769	12.31652	12.31795	12.31441

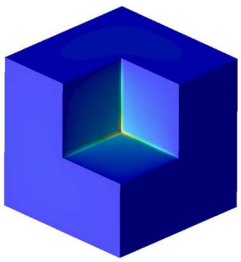

Fig. 7. Modulus of the first eigenfunction (singular).

length 1. This domain contains both a reentrant corner and reentrant edges, and the solutions are strongly singular in the vicinity of these edges and corner. In order to capture the singularities we have defined the domain with seven cubic patches, that are strongly refined toward the corner (see Fig. 6).

The problem has been solved with different degrees and continuities. We present in Table II the results for $p = 3$ in a mesh formed by 875 elements, and for $p = 6$ in a mesh of just seven elements (one element per patch), and its comparison with the ones obtained in [9], where anisotropic edge elements of variable degree were used, and the best ones presented in [10]. Once again, our method requires less degrees of freedom than finite elements to obtain good approximation results. Finally, in Figs. 7 and 8 we draw the modulus of the computed first and fifth eigenfunctions, to show that both singular and analytical solutions are approximated correctly.

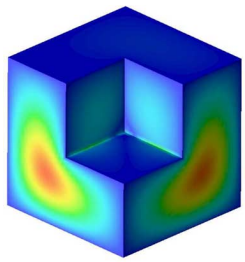

Fig. 8. Modulus of the fifth eigenfunction (nonsingular).

V. CONCLUSION

We have presented the first numerical results for the isogeometric generalization of edge elements. In particular, our technique: 1) is adequate for the optimal treatment of complex geometries; 2) produces regular fields preserving the optimal convergence rates also toward singular solutions. Finally, the main drawback of this technique is the patchwise tensor product structure. We emphasize that local refinement and nonstructured meshes can be obtained by adapting the theory of T-splines [11] to IGA. This goes beyond electromagnetic applications, and it is the object of intense studies.

REFERENCES

[1] R. D. Graglia and G. Lombardi, "Singular higher order complete vector bases for finite methods," *IEEE Trans. Antennas Propagat.*, vol. 52, no. 7, pp. 1672–1685, Jul. 2004.
[2] M. Costabel and M. Dauge, "Weighted regularization of Maxwell equations in polyhedral domains. A rehabilitation of nodal finite elements," *Numer. Math.*, vol. 93, no. 2, pp. 239–277, 2002.
[3] T. J. R. Hughes, J. A. Cottrell, and Y. Bazilevs, "Isogeometric analysis: CAD, finite elements, NURBS, exact geometry and mesh refinement," *Comput. Methods Appl. Mech. Eng.*, vol. 194, no. 39–41, pp. 4135–4195, 2005.
[4] L. Piegl and W. Tiller, *The NURBS Book*, 2nd ed. New York: Springer-Verlag, 1997.
[5] A. Buffa, G. Sangalli, and R. Vázquez, "Isogeometric analysis in electromagnetics: B-splines approximation," *Comput. Methods Appl. Mech. Eng.*, vol. 199, no. 17–20, pp. 1143–1152.
[6] A. Buffa, J. Rivas, G. Sangalli, and R. Vázquez, "Isogeometric analysis in electromagnetics: Theory and testing," *SIAM J. Numer. Anal.*, submitted for publication.
[7] J. C. Nédélec, "Mixed finite elements in R^3," *Numer. Math.*, vol. 35, pp. 315–341, 1980.
[8] M. Costabel and M. Dauge, "Computation of resonance frequencies for Maxwell equations in non-smooth domains," in *Topics in Computational Wave Propagation*. Berlin, Germany: Springer, 2003, vol. 31, Lecture Notes in Computer Science and Engineering, pp. 125–161.
[9] S. Zaglmayr, "High order finite element methods for electromagnetic field computation," Ph.D. dissertation, Johannes Kepler Univ. Linz, Linz, Austria, 2006.
[10] M. Dauge [Online]. Available: http://perso.univ-rennes1.fr/monique.dauge/benchmax.html
[11] Y. Bazilevs, V. M. Calo, J. A. Cottrell, J. A. Evans, T. J. R. Hughes, S. Lipton, M. A. Scott, and T. W. Sederberg, "Isogeometric analysis using T-splines," *Comput. Methods Appl. Mech. Eng.*, vol. 199, no. 5–8, pp. 229–263, 2010.